ARTICLE NO. 79-1563R

Adverse Pressure Gradient Effects on Supersonic Boundary-Layer Turbulence

A. J. Laderman*
Ford Aerospace & Communications Corporation, Newport Beach, Calif.

Measurements of mean flow profiles at several streamwise locations in a supersonic turbulent boundary layer growing under a continuous adverse pressure gradient are reported. Tests are performed at Mach 3 using two curved ramps designed to produce constant pressure gradient, dp/dx, flows, corresponding to $\beta_{k0} = (dp/(dx)(\delta_k^*/\tau_w)_0 = 0.4$ and 1.85, where the ratio of kinematic boundary-layer thickness to wall shear $(\delta_k^*/\tau_w)_0$ is evaluated at conditions upstream of the ramp. The profile data are shown to correlate with the compressible generalization of Coles' universal "wall-wake" velocity profile and they indicate that the boundary layer is in local equilibrium and essentially independent of upstream history. The turbulent transport terms were extracted from the mean flow data and, for a given ramp, show that the distribution of shear stress τ, normalized by the local wall value τ_w, is severely distorted by the pressure gradient although it is insensitive to the local β_k. However, for the several ramps, the peak value of τ/τ_w appears to correlate with β_{k0}. Both the mixing length and the eddy viscosity profiles reflect distortions due to pressure gradient similar to those observed in the shear stress profile.

Nomenclature

C_f = skin friction coefficient, $2\tau_w/\rho_e u_e^2$
G = Clauser shape factor
ℓ = mixing length
M = Mach number
p = pressure
p_t = pitot pressure
R = radius of curvature
Re = Reynolds number
S = streamwise coordinate
T = temperature
u = velocity
u_τ = friction velocity, $(\tau_w/\rho_w)^{1/2}$
u^+ = transformed velocity
W = Coles wake function
x = axial coordinate
y' = coordinate normal to tunnel axis
y = coordinate normal to local surface
y^+ = transformed value of y
β = curvature parameter, $1/(1+y/R)$
β_k = local pressure gradient parameter, $(dp/dx)\ (\delta_k^*/\tau_w)$
β_{k0} = pressure gradient parameter based upon (δ_k^*/τ_w) upstream of ramp
δ = boundary-layer thickness
δ_k^* = kinematic boundary-layer thickness
Δ = Clauser displacement thickness
ϵ = eddy viscosity
$\tilde{\pi}$ = Coles wake strength parameter
ρ = density
τ = shear stress

Subscripts

e = boundary-layer edge
0 = stagnation condition
W = wall condition
∞ = freestream condition

Presented as Paper 79-1563 at the AIAA 12th Fluid and Plasma Dynamics Conference, July 23-25, 1979; submitted Sept. 10, 1979; revision received March 3, 1980. Copyright © American Institute of Aeronautics and Astronautics, Inc., 1979. All rights reserved.

Index categories: Boundary Layers and Convective Heat Transfer—Turbulent; Supersonic and Hypersonic Flow.

*Principal Scientist, Aerothermal Analysis Section. Member AIAA.

Introduction

SOLUTIONS to the supersonic boundary-layer equations require accurate models to describe the turbulent transport of energy and momentum. The transport coefficients cannot be derived from first principles, but must be deduced from well-designed experimental studies. Ideally, it is preferred to measure the turbulence terms directly, e.g., using the hot-wire anemometer, although even in the absence of direct information, the so-called "inverse" or "indirect" method can be applied to extract the transport properties from the detailed mean flow measurements by means of the time-averaged conservation equations. While definite advances have been made for the zero pressure gradient (ZPG), flat-plate boundary layer, there is still a dearth of specific information concerning flows with a finite continuous variation in static pressure. This problem arises from the fact that while numerous experimental studies have been made of boundary layers with pressure gradients (see, e.g., the exhaustive catalog of experimental results compiled by Fernholz and Finley[1]), few have been sufficiently complete and reliable to supply the data required for the turbulence transport model. The situation is compounded in part by the variety of factors characterizing flows with finite pressure gradient which include the usual parameters of Mach number, Reynolds number, and heat transfer as well as the magnitude and rate of change of dp/dx, streamline curvature, pressure gradients normal to the streamlines, etc.

Only recently has progress become evident in deducing the transport properties for adverse pressure gradient (APG) flows.[2-5] In these cases, however, the data was obtained in boundary layers growing over flat or straight walls. For the case of flow over a curved surface, which introduces the effects of streamwise curvature and pressure gradient normal to the surface, direct measurements are not yet available and only Sturek[6] has reported on turbulent shear stresses calculated from mean flow data.

The present study was undertaken, therefore to study systematically the influences of a continuous APG on a two-dimensional, supersonic, adiabatic boundary layer growing over a curved wall. Two constant dp/dx ramps were designed for this purpose, one corresponding to a weak and the other to a moderate pressure gradient. Detailed measurements of the mean flowfield over the ramps were carried out and the results of the data analysis are presented here. In particular, it is

shown that the mean flow profiles, when suitably transformed for compressibility, agree with the universal "wall-wake" velocity profile and that the pressure gradient parameter β_k correlates the data with low-speed results. In addition, the distribution across the boundary layer of turbulent shear stress, mixing length, and eddy viscosity were determined using the 'indirect" method modified by Sturek[6] to account for the effects of longitudinal curvature. A complete description of the experiment and the methods used for data reduction can be found in Ref. 7.

Experiment

The experiment was carried out in the Ford Aerospace & Communications Corporation Mach 3 supersonic wind tunnel, a continuous flow facility with a 7.87×8.64 cm test section located 40.6 cm downstream of the throat section. The turbulent boundary layer at the beginning of the test section is fully developed and is approximately 0.7 cm thick. All tests were conducted for stagnation conditions P_0 and T_0 of 0.973×10^5 N/m^2 and 317 K, respectively, corresponding to a freestream unit Reynolds number $= 6.57 \times 10^6$/m. Two continuously curved ramps, designated ramps 1 and 3, were designed to produce two-dimensional, constant pressure gradient (dp/dx) flows. Based on the boundary-layer characteristics upstream of the ramp leading edge, the pressure gradient parameter $\beta_{k0} = (\delta_k^*/\tau_w)_0 (dp/dx)$ was nominally 0.4 and 1.85 for ramps 1 and 3, respectively. The ramp contours and a sketch of the ramp installed in the wind-tunnel test section are indicated in Fig. 1. The ramp models were designed to replace the floor plate of the wind-tunnel test section and to provide a smooth continuation of the lower nozzle block. Each ramp was provided with 0.084 cm diameter pressure ports aligned along the ramp centerline at 1.27 cm intervals. The measured surface pressure distributions for the two ramp models are shown in Fig. 2, which also includes data obtained from the static pressure surveys discussed later. In both cases, the measured pressure increase is sufficiently linear that the flow can be considered as characterized by a constant pressure gradient with dp/dx equal to 16,000 and 66,600 N/m^3 for ramps 1 and 3, respectively. Prior to the conduct of the final measurements, detailed pressure surveys were carried out to insure two-dimensional, disturbance-free flow over the ramps. These surveys provided evidence that the flow was two-dimensional with negligible cross-flow effects and free of the longitudinal vortices that have been observed in subsonic flow over concave surfaces.

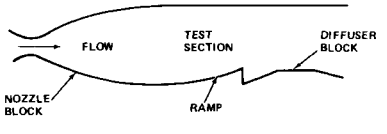

SCHEMATIC OF WIND TUNNEL SHOWING RAMP INSTALLATION

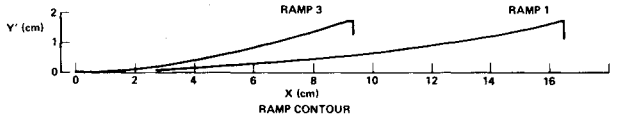

RAMP CONTOUR

RAMP 1		RAMP 3	
X (cm)	Y'(cm)	X (cm)	Y' (cm)
2.736	0.076	1.27	0.0475
4.006	0.142	2.54	0.176
5.276	0.225	3.81	0.372
6.439	0.316	5.08	0.626
7.709	0.430	6.35	0.933
8.979	0.559	7.62	1.289
10.249	0.703	8.89	1.689
11.519	0.861	9.144	1.774
12.789	1.033		
14.059	1.219		
15.329	1.409		

Fig. 1 Schematic of ramp contours and wind-tunnel installation.

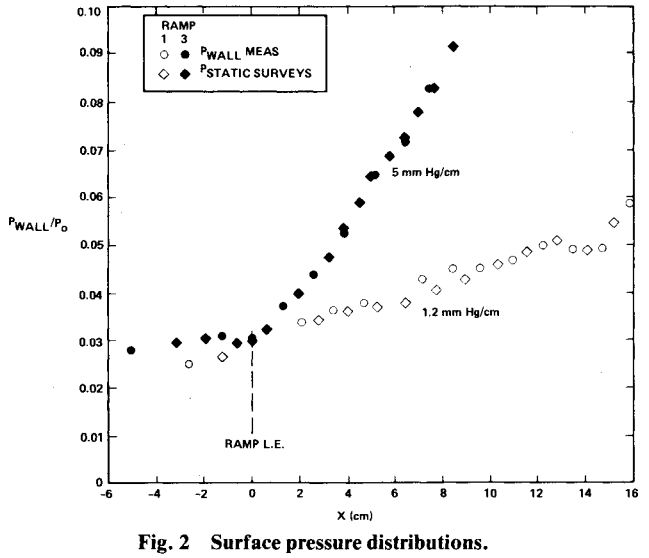

Fig. 2 Surface pressure distributions.

Measurements were made of mean profiles of pitot pressure, static pressure, and recovery temperature across the boundary layer using calibrated miniaturized probes. Each probe was remotely driven and mounted in the tunnel separately to avoid any possibility of mutual interference between probes and to minimize blockage by the presence of the probes. For both probes, various corrections due to rarefaction and viscous effects were found to be negligible. With the pitot probe, an interference effect, caused by proximity of the surface, was observed for positions very close to the wall. These effects, however, were very small and restricted to, at most, a few positions and therefore no corrections were made. In addition, the static pressure profiles indicated a small (10%) interference effect near the surface of the ramp which extended out to about $y^1 = 0.12$ cm. Since the static pressure varied nearly linearly through the remainder of the boundary layer, it was possible to correct for the interference effect by extrapolating the static pressure profile to the wall. This permitted a redundant determination of the surface pressure distribution. These results are shown in Fig. 2 where they are seen to provide excellent agreement with the direct measurements of wall pressure. Although the ramps were not instrumented to measure surface temperature, on the basis of a similar boundary layer study[8] performed in the same facility, it was assumed that $T_w = 0.945\ T_{0_e} = 300$ K which corresponds essentially to the adiabatic wall condition. Measurement of wall shear stress was made using a 0.01 cm o.d. Preston tube.

Profile data were acquired by first locating the probe adjacent to the ramp surface where the surface was located using a 10-power microscope with a calibrated graticle. The probe was then moved vertically upward (normal to the tunnel centerline) with data acquired at intervals of 0.5-5 mils.

Data Reduction

The data reduction procedure was computer programmed and all data processing was carried out via a time-share terminal. At each survey station, the pitot pressure, static pressure, and recovery temperature profile data were combined to form a single data file. Since the y^1 positions for the static pressure and recovery temperature profiles differed from those for the pitot pressure survey, the data for the former was interpolated to provide static pressure and recovery temperature data at the same y^1 locations as the pitot pressure. Mean flow properties were calculated then by means of standard gasdynamic equations using an iterative procedure to account for the calibrated recovery temperature characteristics of the T_0 probe.

For each ramp, the profiles measured along the vertical were converted to profiles along the normal to the surface using a simple four-point interpolation scheme. At a given station, the interpolation was carried out using profile data

along the vertical at that station together with vertical profile data at the nearest upstream station. The interpolated flowfield, which consisted of profiles along the normal at all x stations, was stored in a single data file for subsequent manipulation.

As shown later, the streamwise derivatives of the flow variables u, ρu, ρu^2, and p are needed to extract the turbulent transport properties from the mean flow data. To accomplish this, an x survey station is selected as a reference location and the associated y values are denoted as y_0. The remaining profiles are then interpolated to find $u(s,y_0)$, $\rho u(s,y_0)$, etc. The streamwise distance s at y_0 is easily determined knowing the axial location x of the survey station and the local surface curvature. For each y_0, the flow properties are curve-fit by the method of least squares to the expression:

$$F(s,y_0) = F_1 + F_2 s + F_3 s^2$$

where $F = u$, ρu, ρu^2, or p. With F_1, F_2, and F_3 specified, the streamwise derivatives are easily determined. Once the derivatives are found at a given profile station, the shear stress distribution τ/τ_w vs y_0, together with the mixing length and eddy viscosity, can be computed.

Experimental Results

Characterization of the Pressure Gradient

In his treatise on the incompressible turbulent boundary layer, Clauser[9] concluded that the proper parameter to use for characterizing equilibrium profiles in a flow with pressure gradient is $\beta = (\delta^*/\tau_w)\mathrm{d}p/\mathrm{d}x$. For compressible flows, Alber and Coats[10] suggested replacing β with $\beta_k = (\delta_k^*/\tau_w)\mathrm{d}p/\mathrm{d}x$ and in their study at $M_\infty = 4$, Lewis et al.,[11] found that using β_k does provide an improved correlation with the low-speed data. For the present experiment, the variation of β_k with axial position x is plotted in Fig. 3. It is shown later that τ_w increases with x much faster than δ_k^* and, since $\mathrm{d}p/\mathrm{d}x$ is a constant, then, as indicated in Fig. 3, β_k decreases in the axial direction, particularly for ramp 3. Figure 3 includes the data of Sturek and Danberg[12-14] which were obtained for a constant $\mathrm{d}p/\mathrm{d}x$ using a curved ramp similar to that involved in the present tests. While a direct comparison cannot be made since the axial coordinate x has not been properly normalized, their data also show that β_k decreases with increasing x, confirming the present findings. Furthermore, the magnitude of β_k in their experiments indicates that the relative influence of their pressure gradient should be much larger than in the present case. This point is addressed later in this report. The data of Lewis et al.,[11] are also shown in Fig. 3 to demonstrate the similarity in the magnitude of the pressure gradient parameter β_k with the present results. Since their test was carried out for an increasing pressure gradient $\mathrm{d}p/\mathrm{d}x$, their values of β_k increase in the streamwise direction. However, the authors demonstrate that their boundary layer is in local equilibrium, i.e., characterized by local conditions only, and that upstream history and variations in β_k have no appreciable effect. Reference to the results of Lewis et al.,[11] will be made in the next section when the present data are compared with the low-speed correlations.

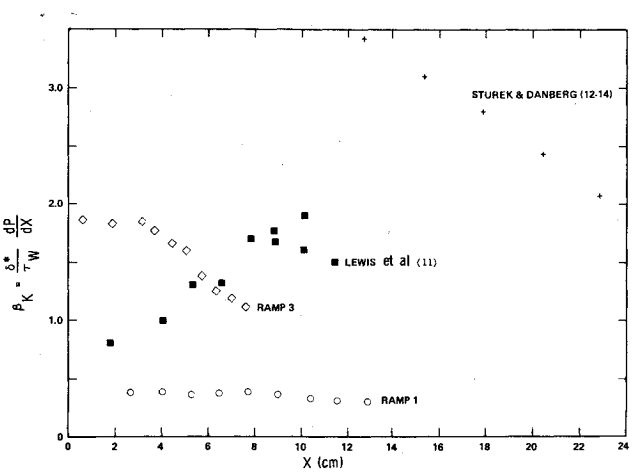

Fig. 3 Streamwise variation of pressure gradient parameter β_k.

Correlation of Velocity Profiles

It has become common practice to compare experimentally measured velocity profiles to a well-defined law (e.g., Coles' composite "wall-wake" correlation[15]) that describes the behavior of an equilibrium turbulent boundary layer. The extension of Coles' incompressible correlation to compressible flows was first carried out by Van Driest[16] for the ZPG case. Subsequently verification of the compressible form of the "wall-wake" law for pressure gradient flows was provided by Mathews et al.[17] Comparison of the data with a "universal" expression for the velocity profile permits an assessment of the quality of the data, represents a means for evaluating the characteristic boundary layer parameters (e.g., δ, c_f, etc.), and in the nonconstant pressure case, assists in identifying the effects of pressure gradient on the development of the boundary layer and provides a basis for comparison with other experiments. The "wall-wake" universal profile is given by

$$u^+ = (1/k)\ell n y^+ + C + (\bar{\pi}/k)\,W(y/\delta) \tag{1}$$

where $\bar{\pi}$ is a parameter representing the strength of wake component of the boundary layer, W is Coles' tabulated wake function which can be approximated by $2\sin^2(\pi y/2\delta)$, the constants k and C are given by their incompressible values 0.41 and 5.0, respectively, and, to avoid reliance on analytical transformations and their approximations, u^+ is defined by

$$u^+ = \int_0^u \left(\frac{\rho}{\rho_w}\right)\frac{\mathrm{d}u}{u_\tau} \tag{2}$$

which arises directly from the conventional mixing length expression. Equation (1) contains three unknowns; u_τ, δ, and $\bar{\pi}$. Substituting the edge conditions into Eq. (1) yields an expression for $\bar{\pi}$ in terms of u_τ and δ. This relation is then substituted into Eq. (1), reducing the number of unknowns to two, whose values are adjusted until the data fit the equation such that the rms error is minimum. Data near the wall and at the outer edge of the boundary layer are excluded from the curve fit and only data for which $y^+ \geq 50$ and $y/\delta \leq 0.9$ are used to determine the boundary-layer parameters.

A typical plot of the experimental velocity profiles in transformed coordinates is shown in Fig. 4 for ramp 1. The dashed lines in Fig. 4 represent the transition or buffer region velocity profile suggested by Spalding.[18] For clarity, a plot of Eq. (1) has been omitted since the differences between the experimental values of u^+ and the theoretical values cannot be resolved within the scale used in the figure. In the region $y^+ < 50$, the data for $\mathrm{d}p/\mathrm{d}x > 0$ tend to lie above the theoretical curve (a feature common to a considerable body of experimental data) with the discrepancy reaching a maximum in the range $10 < y^+ < 20$. This portion of the velocity profile has been replotted to a larger scale in Fig. 5 where for each ramp data from the $\mathrm{d}p/\mathrm{d}x = 0$ survey station and the most farthest downstream station on the ramp have been included, together with the univesal profiles. The $\mathrm{d}p/\mathrm{d}x = 0$ data for ramp 1 is seen to be in excellent agreement with Ref. 18, while for ramp 3, the data lie slightly above those of Ref. 18. In addition, it is observed that when $\mathrm{d}p/\mathrm{d}x > 0$, then for both ramps there is a small but definite increase in the discrepancy between the experimental u^+ and Ref. 18 in the streamwise direction. The reason for this is not immediately obvious, but it is reflected in the mixing length calculations discussed later.

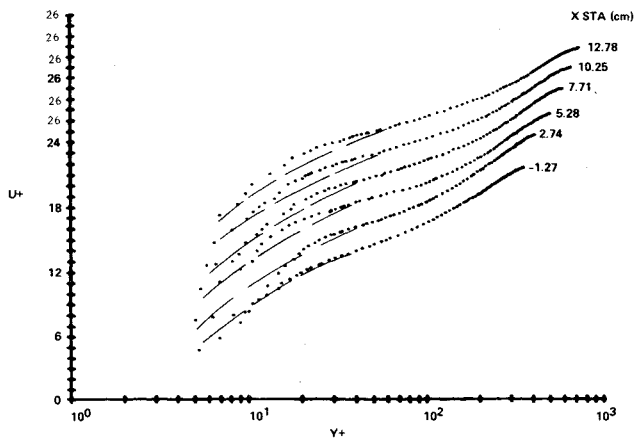

Fig. 4 Typical "law-of-the-wake" velocity correlations, ramp 1.

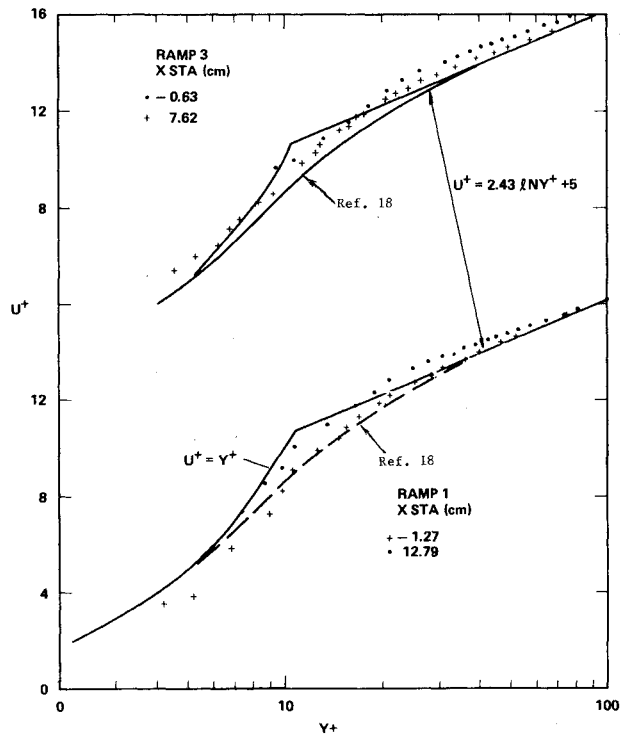

Fig. 5 Velocity correlations in vicinity of $y^+ = 10$.

Clauser[9] defines an effective displacement thickness of the turbulent boundary layer in terms of the transformed velocities as:

$$\Delta = -\delta \int_0^\infty (u^+ - u_e^+) \, d(y/\delta) \tag{3}$$

and the corresponding shape factor as:

$$G = \int_0^\infty (u^+ - u_e^+)^2 \, d(y/\Delta) \tag{4}$$

where for constant pressure layers G and Δ/δ have the values 6.8 and 3.6, respectively. Written in the velocity defect form used in Eq. (3), Eq. (1) becomes:

$$u^+ - u_e^+ = (1/k) \ell n y/\delta - (\tilde{\pi}/k)(W-2) \tag{5}$$

Typical plots of $u^+ - u_e^+$ vs y/Δ for survey stations located just upstream, at the midpoint, and at the rear of the ramp are shown in Fig. 6 for ramp 3 in order to illustrate the effect of the pressure gradient on the shape of the velocity profile. For ramp 3, the velocity profile is initially distorted (compare $x = 5.08$ cm station to $x = 0$ cm station). However, since β_k decreases with x, the effect of the pressure gradient diminishes and the shape of the velocity profile at the rear of the ramp is almost identical to that where $dp/dx = 0$. For ramp 1, the pressure gradient is relatively weak and β_k is nearly constant and the velocity profiles are independent of streamwise location.

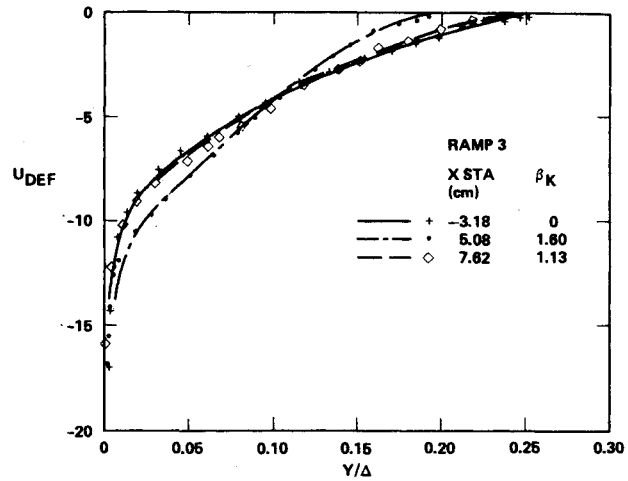

Fig. 6 Velocity deficit form of velocity profiles.

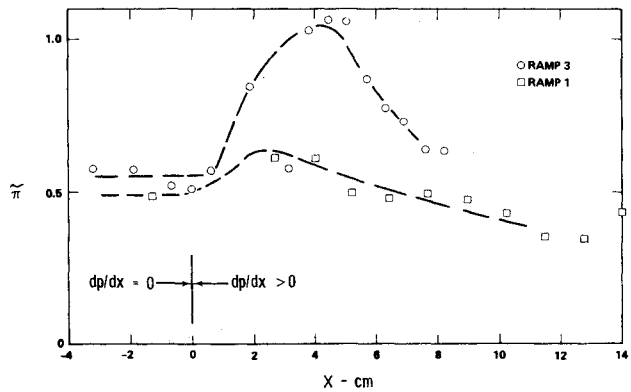

Fig. 7 Streamwise variation of "wake strength parameter."

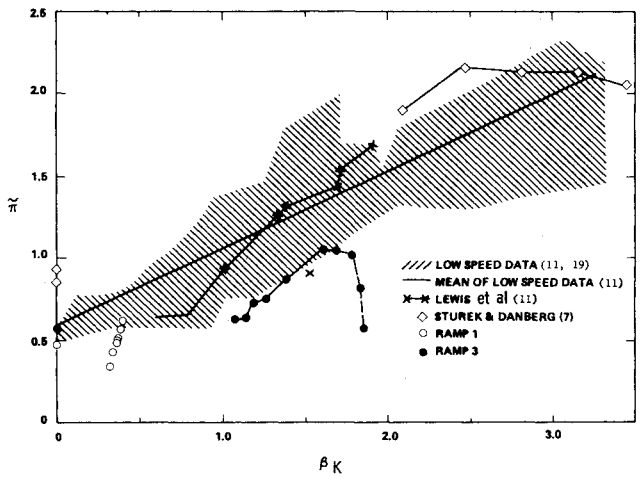

Fig. 8 Correlation of wake parameter $\tilde{\pi}$ with pressure gradient parameter β_k.

Figure 7 presents a plot of the wake parameter $\bar{\pi}$ vs axial station x. For both ramps, $\bar{\pi}$ jumps to a peak value then, similar to β_k, decreases as the rear of the ramp is approached. However, while β_k is maximum at the leading edge of the ramp, the variation of $\bar{\pi}$ with x in this region is much slower, with $\bar{\pi}$ not reaching its maximum value until $x=3$ or 4 cm. Since the pressure waves generated by the curved ramp surface are swept downstream, then just behind the leading edge of the ramp the outer portion of the boundary layer retains a memory of its upstream history (i.e., the flow here is still characteristic of $dp/dx=0$). This is also the wake portion of the boundary layer which contributes largely to the value of $\bar{\pi}$. Therefore, just downstream of the leading edge, the boundary layer is not in equilibrium with the local value of β_k. (Strictly speaking, the procedure for curve-fitting the data to the "law-of-the-wake" is not valid for these first few survey stations since the velocity correlation is restricted to equilibrium flows.) This is indicated in Fig. 8 where $\bar{\pi}$ is plotted vs β_k. The lack of correlation between $\bar{\pi}$ and β_k at the first two ramp survey stations for ramp 3 is quite apparent. Figure 8 also includes the data of Sturek and Danberg[12-14] and Lewis et al.[11] and the results of a number of low-speed experiments examined by Coles and Hirst[19] and correlated by Lewis et al.[11] Interestingly enough, the data of Sturek and Danberg lie near the upper boundary to the spread of the low-speed data, while those of the present tests fall near the lower boundary of the low-speed data. For ramp 1, the values of β_k are too small to identify any specific trend of $\bar{\pi}$ with β_k.

A plot of Clauser's[9] shape factor G vs β_k is shown in Fig. 9. Again, the present data for ramp 3 lie near the lower boundary of the spread of the low-speed data, although the general trend of increasing G with increasing β_k is apparent. The results for ramp 1 lie within the low-speed data spread while, for comparison, the results of Lewis et al.[11] are near the upper boundary of the low-speed data and are in slightly better agreement with the theoretical results of Mellor and Gibson.[20] Excluding the flow just downstream of the ramp leading edge, the results shown in Figs. 8 and 9 are in good agreement with the earlier findings of Lewis et al.,[11] namely, that the boundary layer is in approximately local equilibrium throughout the adverse pressure gradient region. Thus, the boundary-layer profiles are characterized by local conditions only, i.e., G and β_k, unaffected by the fact that these parameters are not constant.

A plot of the wall shear stress τ_w, determined from the curve-fit to the "law-of-the-wake," vs axial station is shown in Fig. 10 which includes wall shear measurements made with the 0.1 cm diameter Preston tube and evaluated using the Bradshaw-Unsworth[21] correlation. The two sets of results are in very good agreement, although the Preston tube measurements are generally lower than the data obtained from the velocity correlation with a maximum difference of 9% at the rear of ramp 3. Both results, however, show a continuous increase in τ_w in the downstream direction. To be consistent with the selection of the boundary-layer thickness δ, the wall shear stress determined from the curve-fit to Eq. (1) is used subsequently in this report. A plot of the local skin friction coefficient $c_f=2\tau_w/\rho_e u_e^2$ vs Re_θ is presented in Fig. 11 which includes, for comparison, the skin friction coefficient for $dp/dx=0$ calculated from the Karman-Schoenherr equation together with the Van Driest transformation as outlined in Hopkins and Inouye.[22] For a given M_e and Re_θ, the maximum deviation between the measured c_f and that calculated for $dp/dx=0$ is about 10% with the measured values somewhat larger.

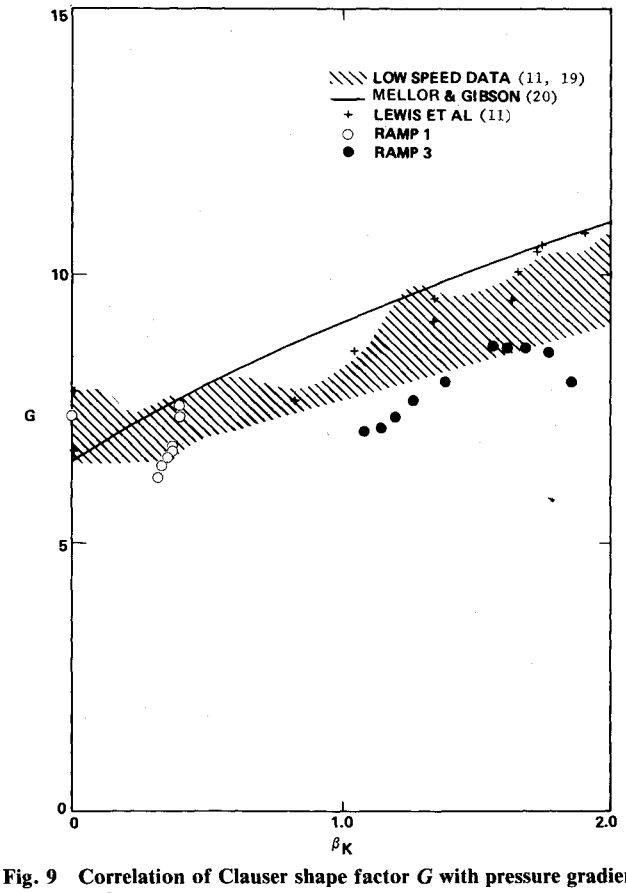

Fig. 9 Correlation of Clauser shape factor G with pressure gradient parameter β_k.

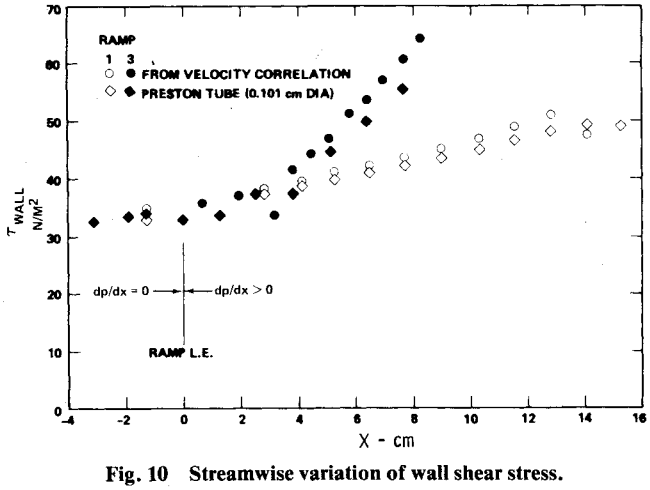

Fig. 10 Streamwise variation of wall shear stress.

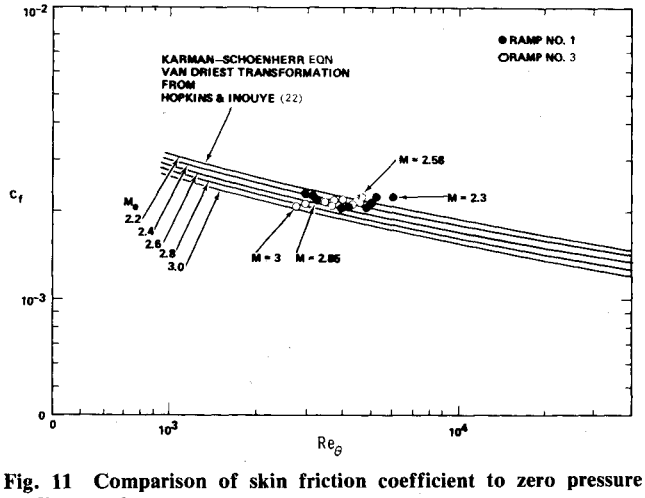

Fig. 11 Comparison of skin friction coefficient to zero pressure gradient results.

Turbulent Shear Stress Distribution

The calculation of turbulent shear stress from mean flow profiles was apparently first attempted by Coles,[23] who also identified the closure problem at the boundary-layer edge which is discussed later. In the present case combining the continuity and streamwise momentum equations for a ZPG, adiabatic boundary layer and making the assumption of local similarity, the distribution of shear stress across the boundary layer can be expressed as:

$$\frac{\tau}{\tau_w} = 1 + \frac{1}{\theta \rho_\infty u_\infty^2}\left(\int_0^y \rho u^2 dy - u\int_0^y \rho u dy\right) \tag{6}$$

which can be evaluated numerically using the measured profile data.

Sturek[6] has developed the equations of continuity and momentum conservation for a two-dimensional boundary layer over a surface with longitudinal curvature. Integrating these expressions in the direction y normal to the surface and combining the resulting equations yields the following relation for the shear stress distribution:

$$\frac{\tau}{\tau_w} = 1 + \frac{1}{\tau_w}\left\{\int_0^y \beta \frac{\partial}{\partial s}(\rho u^2)dy - u\beta\int_0^y \frac{\partial}{\partial s}(\rho u)dy - 2\int_0^y \left(\int_0^y \frac{\partial}{\partial s}(\rho u)dy\right)\frac{u\beta^2}{R}dy + \int_0^y \beta \frac{\partial p}{\partial s}dy\right\} \tag{7}$$

The streamwise derivatives $\partial/\partial s$ appearing in the above equation were determined using the curve-fit procedure described in the previous section, and the values of the wall stress τ_w were taken from the correlation of the measured profile data with Coles' "law-of-the-wake." Equation (7) includes terms which represent the effects of streamwise curvature and while their contribution can be shown to be small, they are the same order of magnitude as the wall stress and, therefore, have been retained. However, neither the velocity correlation described earlier nor the analysis which follows indicates any influence on the results due to curvature other than that introduced by the pressure gradient.

The computed normalized shear stress distribution for ramp 1 are shown in Fig. 12 and include the stress distribution in the ZPG region 1.27 cm upstream of the ramp leading edge and those obtained in the APG region of stations at $x = 5.27$-12.79 cm. The scatter in the data points is nil and for clarity, the shear stress distributions have been represented by continuous lines drawn through the data points. In the ZPG case, the computed shear stress distribution is in good agreement with expectations based upon Sandborn's "best estimate" for flat-plate boundary layers.[24] For the APG region, the stress distributions indicate a peak at $y \approx 0.2$-0.3 cm ($y/\delta \approx 0.3$-0.45), with the location at the peak value shifting away from the wall at the downstream locations. In addition, the shear stress remains finite at the edge of the layer although there is a systematic shift in the sign of the residual τ from negative to slightly positive in the downstream direction.

If the data input to Eq. (7) were completely accurate, the shear stress should tend to zero in the external flow. (Actually, the flow in the external stream is not uniform, so that the streamwise derivatives there do not identically vanish and τ remains finite, albeit small.) Even if the measured profiles were highly accurate, each of the subsequent manipulations to which the data is subjected introduces an uncertainty which reflects in the final results. Thus, the nonvanishing stress at the boundary layer edge in Fig. 12 is believed to be primarily a consequence of the data processing. It is possible to "correct" the data so that the shear stress does vanish at the edge of the boundary layer. For example, Sturek[6] altered his profile of $\partial \rho u/\partial s$ vs y to eliminate a large negative residual stress at $y/\delta = 1.0$. However, there is no rationale for changing only one of the derivative terms to the exclusion of the others. It is also possible to alter the curve-fit by excluding some of the profile stations, although there is no basis for culling the data used in the curve-fit except for that just behind the leading edge. Consequently, the data has been left unaltered and the shear stress distributions at x stations 8.98, 10.25, and 11.52 cm, where τ/τ_w becomes negligible at the edge of the boundary layer, are considered representative of ramp 1.

Since the flow properties from $y = 0$ to $y = y$ all contribute to the magnitude of τ at $y = y$, any correction which would cause $\tau \to 0$ at $y = \delta$ would also introduce a change of the same sign and a magnitude proportional to the peak shear stress. In Fig. 12, it appears that if τ was adjusted to vanish at the edge of the layer, then the stress distributions τ/τ_w vs y/δ tend to approach each other. This implies that the normalized shear stress distribution is insensitive to the x location, i.e., to β_k, and is instead dependent upon dp/dx. The results show further that even a weak pressure gradient $\beta_k \approx 0.4$ produces a peak shear stress 60% greater than the wall shear.

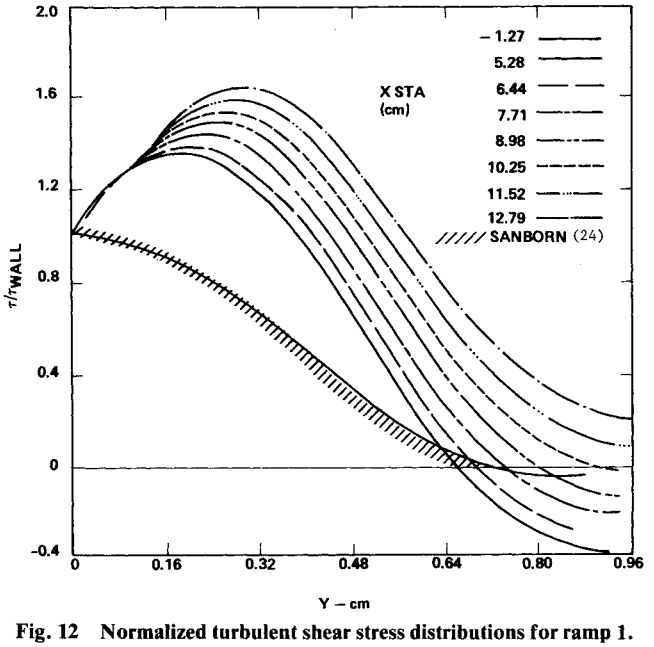

Fig. 12 Normalized turbulent shear stress distributions for ramp 1.

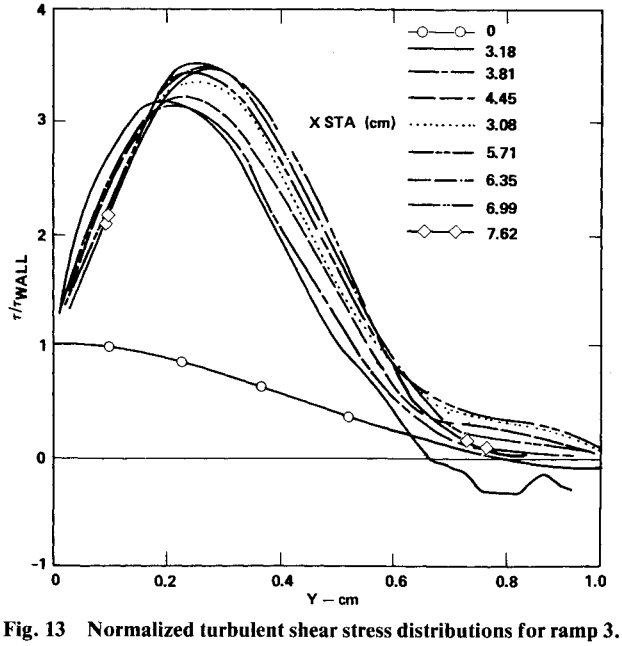

Fig. 13 Normalized turbulent shear stress distributions for ramp 3.

The shear stress distributions for ramp 3 are shown in Fig. 13 which includes again the ZPG result and the results for survey stations in the adverse pressure region $x=3.18$-7.62 cm. While the peak shear stress in this case is 3-3.5 times the wall value, the behavior of the stress distribution as a function of x is similar to that observed for ramp 1 and most of the comments made concerning the ramp 1 results apply to ramp 3 as well. In particular, the shear stress does not vanish completely at the edge of the boundary layer (although $\tau \to 0$ in the external stream). The residual shear stress at $y \sim \delta$ is generally positive with a maximum absolute value of $0.4\,\tau_w$, which is probably the maximum uncertainty introduced by the data processing, and is now only 10% of the maximum shear stress in the boundary layer. These data show more conclusively that the normalized shear stress distribution appears to be dependent upon dp/dx rather than β_k which, for this ramp, decreases by a factor of almost two in the streamwise direction. Sturek's[6] results indicate a relaxation effect on the shear stress profile since the maximum τ/τ_w at his forward survey station (which was located near the midpoint of his ramp) was one-half the peak τ/τ_w observed at his downstream stations. However, in his case, dp/dx varied continuously from 0 to a finite value at the forward survey station where it remained constant over the remainder of the ramp. This contrasts the present experiment where a constant dp/dx was imposed at the ramp leading edge and may account for his observations. It should also be noted that the peak τ/τ_w increased quickly downstream of his first survey station.

The effect of pressure gradient on the turbulent shear stress distribution across the boundary layer is illustrated in Fig. 14 where stress profiles τ/τ_w vs y for $dp/dx=0$ and representative stations of ramps 1 and 3 are shown. It is apparent that the stress distribution is extremely sensitive to dp/dx with the peak value of τ/τ_w rising from 60 to 300% above the wall value for the weak-to-moderate pressure gradients used in the present tests. It should be emphasized that while τ/τ_w vs y is invariant with x location, the absolute magnitude of τ is increasing since τ_w increases with x.

Since β_k is a decreasing function of x for a constant pressure gradient flow, it cannot be used to correlate the shear stress τ/τ_w which appears to be insensitive to x. However, the parameter β_{k0}, where δ_k^* and τ_w are evaluated in the ZPG flow just upstream of the curved surface, is a characteristic of the flowfield and remains constant for constant dp/dx. A plot of the peak value of τ/τ_w vs β_{k0}, including data from Sturek's[6,12] experiment and the present tests, is shown in Fig. 15. The dashed line representing a linear variation of $(\tau/\tau_{wall})_{max}$ with β_{k0} was drawn through the most representative values of $(\tau/\tau_{wall})_{max}$ obtained from the present tests. Although the data do not follow a linear variation, they indicate a consistent trend and demonstrate a reasonable agreement between the results of the two experiments.

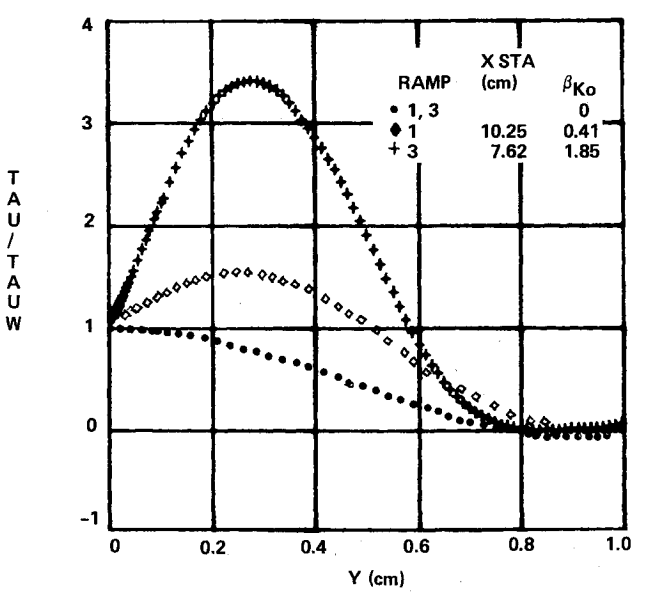

Fig. 14 Effect of pressure gradient on normalized turbulent shear stress distribution across boundary layer.

Turbulent Transport Coefficients

With the turbulent shear stress distribution determined, it is possible to calculate the mixing length ℓ and the eddy viscosity ϵ, using the following expressions:

$$\frac{\ell}{\delta} = \left[\frac{\tau/\rho_e u_e^2}{(\rho/\rho_e)\,[\partial(u/u_e)/\partial(y/\delta)]^2}\right]^{1/2} \tag{8}$$

$$\frac{\epsilon}{u_e \delta_k^*} = \frac{\tau/\rho_e u_e^2}{(\rho/\rho_e)\,[\partial(u/u_e)/\partial(y/\delta)]\,(\delta_k^*/\delta)} \tag{9}$$

In the above expressions, τ is the turbulent shear stress and is obtained by subtracting from the stresses computed in the previous section the laminar contribution $\mu \partial u/\partial y$. Because of the very high density of data points, $\partial u/\partial y$ was determined directly from the measured velocity profile using a simple differencing scheme and no attempt was made to smooth either the velocity profile or the variation of $\partial u/\partial y$. Near the outer edge of the boundary layer, both τ and $\partial u/\partial y$ tend toward zero. As a consequence, large errors are introduced in the calculation of $\epsilon/u_e\delta_k^*$ and, particularly, in ℓ/δ. For this reason, when $y/\delta > 0.8$ these quantities are considered unreliable and are not included in the results.

A plot of ℓ/δ vs y/δ for the ZPG boundary layer upstream of ramp 3 is shown in Fig. 16. The scatter in the data, while not small, does not detract from a well-defined trend. Both

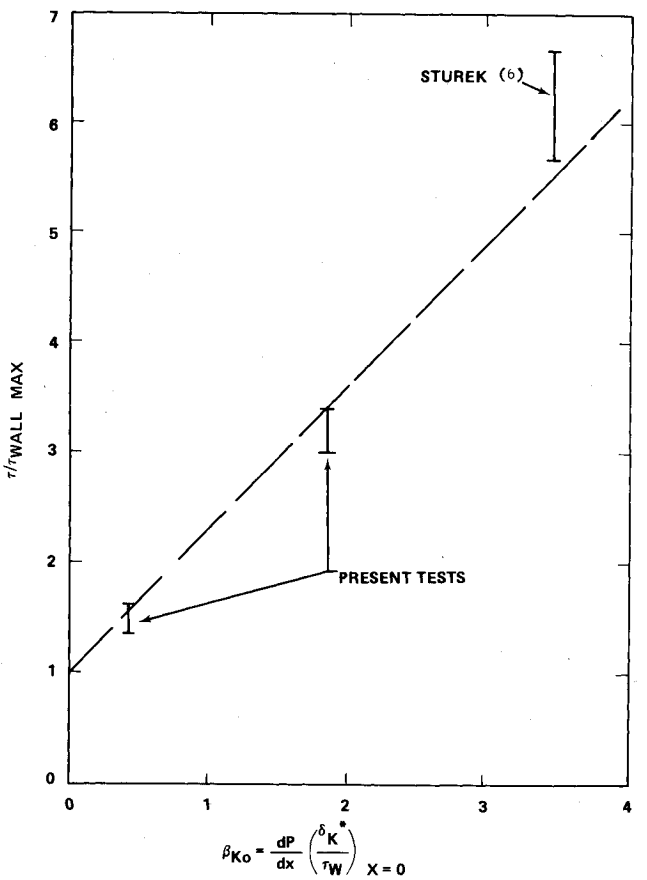

Fig. 15 Variation of peak shear stress τ/τ_w with pressure gradient parameter β_{k0}.

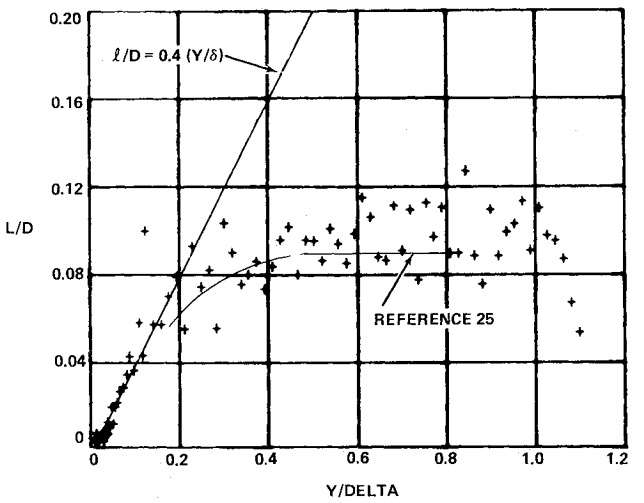

Fig. 16 Distribution of mixing length ℓ/δ across boundary layer for zero pressure gradient flow.

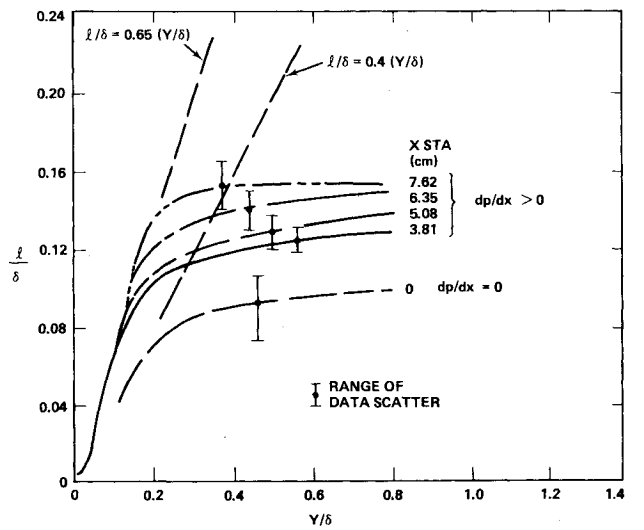

Fig. 17 Effect of adverse pressure gradient on mixing length, ramp 3.

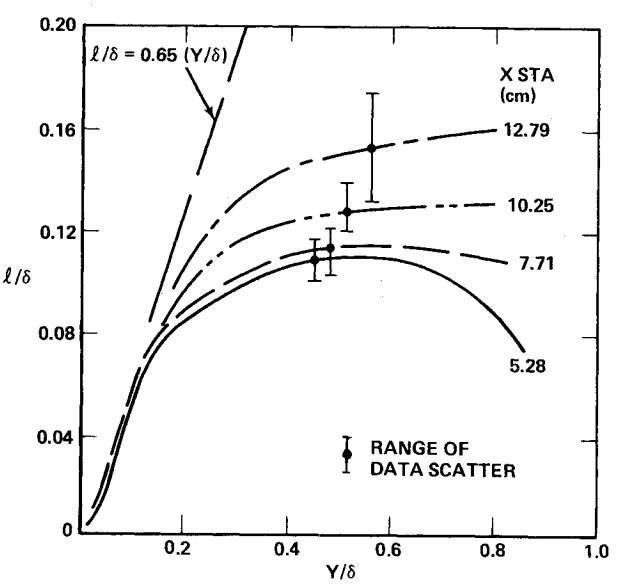

Fig. 18 Effect of adverse pressure gradient on mixing length, ramp 1.

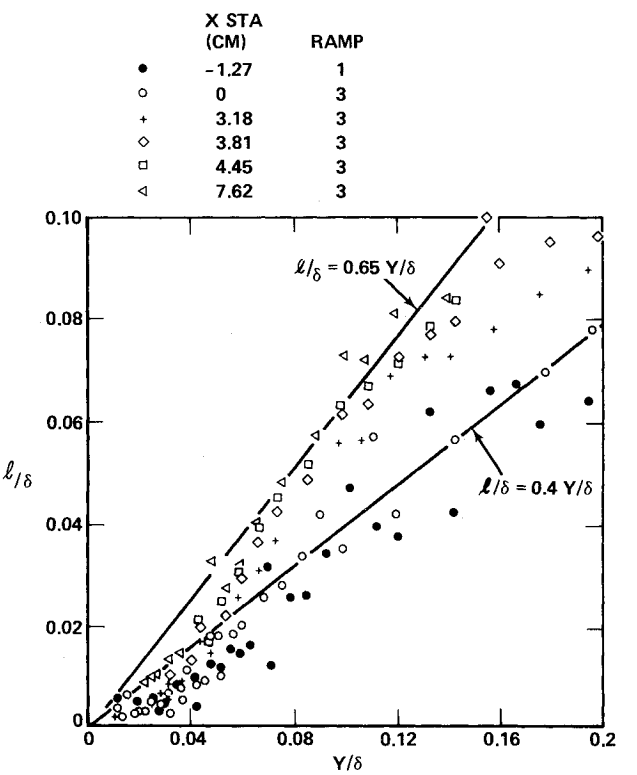

Fig. 19 Variation of mixing length ℓ/δ with position y/δ in wall region.

the slope of the data in the wall region ($\ell/\delta = 0.4\, y/\delta$) and the magnitude of ℓ/δ in the plateau region are in good agreement with the conventionally accepted results of Maise and McDonald.[25] The influence of the adverse pressure gradient on ℓ/δ is shown in Figs. 17 and 18 for ramps 3 and 1, respectively. Because of the scatter in the results, the variation of ℓ/δ with y/δ has been represented by a curve drawn through the mean of the data points and the maximum range of the scatter is denoted by a vertical bar on each mean curve. While τ/τ_w was shown to be insensitive to x, the mixing length is not normalized by a wall parameter and, therefore, ℓ/δ is dependent upon the x station and increases in the downstream direction.

Two points of particular interest are apparent in Figs. 17 and 18. First, in the APG region, the slope $k(\ell/\delta = ky/\delta)$ in the wall region is 0.65 instead of the conventional value of 0.41, and is independent of x and dp/dx. This finding, illustrated more clearly in Fig. 19, is similar to that inferred by Bradshaw and Ferris[26] from their hot-wire measurements in an incompressible flow over a flat wall with $\beta_k = 5$. The data of Bradshaw and Ferris and that from other incompressible experiments have been analyzed by Glowacki and Chi[27] and by Galbraith and Head[28] who concluded that k is indeed dependent upon pressure gradient and appears to increase with β_k. The present compressible results indicate that k is insensitive to β_k and, in fact, the value $k = 0.65$ is identical to Sturek's[6] observation for $\beta_{k0} = 3.5$. Although beyond the scope of the present paper, the fact that $k > 0.41$ for APG flows impacts directly on the values of the constants used in the "law-of-the-wall" correlation. In particular, it accounts for the discrepancy between the data and the correlation noted in Fig. 5. Second, the magnitude of ℓ/δ in the plateau, or outer region, is similar to the values found by Sturek,[6] although Sturek's value of β_{k0} and that for ramps 1 and 3 differ by as much as a factor of 9.

A plot of the normalized eddy viscosity $\epsilon/u_e\delta_k^*$ vs y/δ for the same $dp/dx = 0$ station shown in Fig. 16 is presented in Fig. 20 where it is found to be in excellent agreement with the

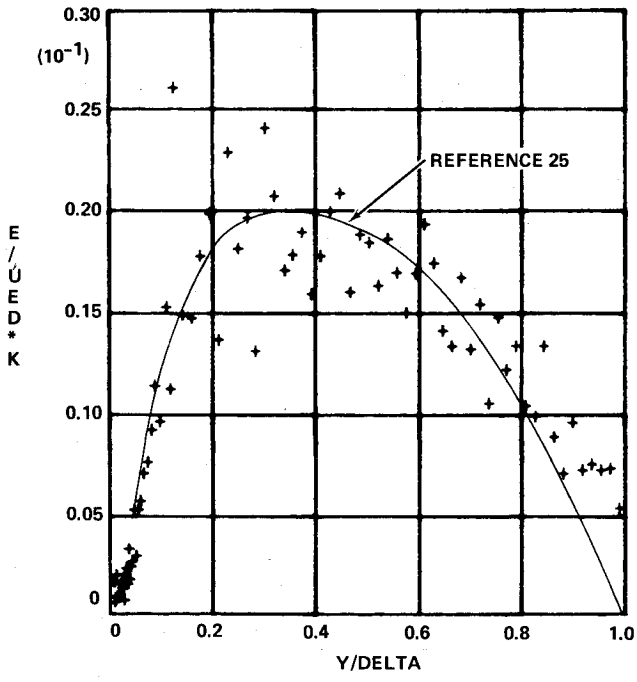

Fig. 20 Variation of normalized eddy viscosity with y/δ for zero pressure gradient flow.

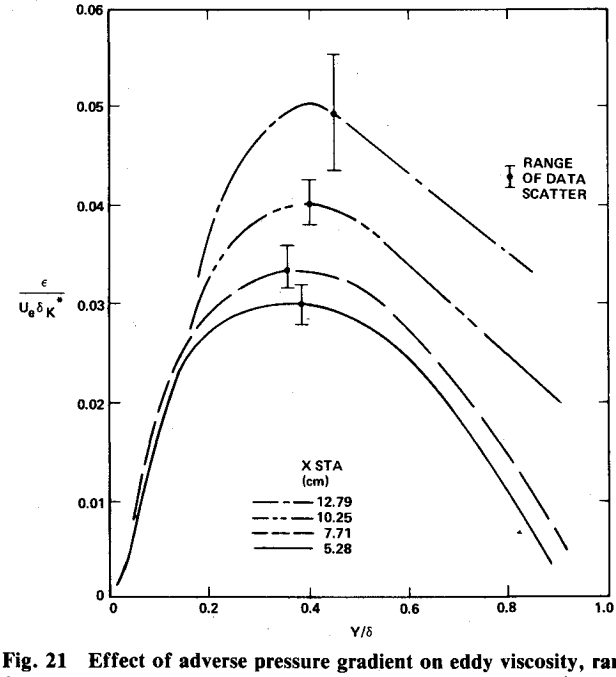

Fig. 21 Effect of adverse pressure gradient on eddy viscosity, ramp 1.

universally accepted results of Maise and McDonald[25] for a similar M_∞ and Re_θ. The effect of adverse pressure gradient on the eddy viscosity is shown in Figs. 21 and 22 where, similar to the mixing length, the data points have been replaced by continuous curves faired through the points and the maximum scatter in the data is represented by vertical bars. These figures reflect the same behavior observed for the mixing length and show that the eddy viscosity increases with x, with somewhat larger increases apparent for the larger value of dp/dx. In fact, the maximum value of $\epsilon/u_e\delta_k^*$ is even larger than that found by Sturek[6] although Sturek's value of β_{k0} is twice as large as that for ramp 3. However, for the ZPG case, Sturek found $\epsilon/u_e\delta_k^*$ to be only half as large as that predicted by Maise and McDonald[25] and this discrepancy may also be reflected in his adverse pressure gradient results.

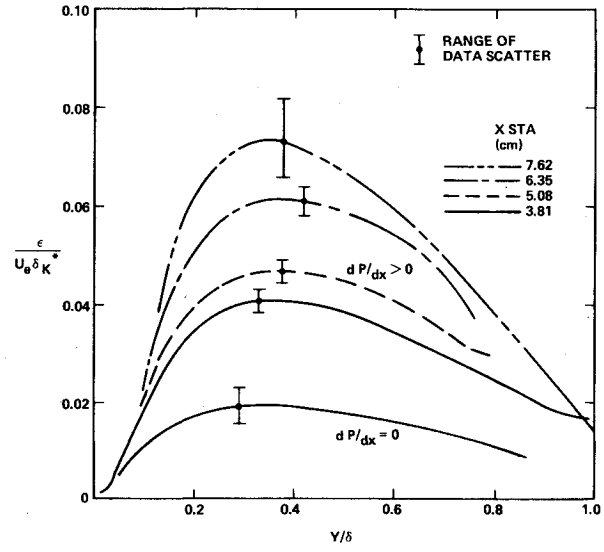

Fig. 22 Effect of adverse pressure gradient on eddy viscosity, ramp 3.

Summary

Measurements have been made of mean flow profiles at several streamwise locations in the supersonic turbulent boundary layer over several curved ramp surfaces. Analysis of the profile data indicates that with an appropriate compressibility transformation, the data correlate with the well-defined Coles' "wall-wake" incompressible velocity profile. In addition, correlation of the wake parameter $\tilde{\pi}$ and the Clauser shape factor G with the local pressure gradient parameter β_k is in agreement with the low-speed data. Finally, similar to the earlier findings of Lewis et al.,[11] the boundary layer appears to be in a state of local equilibrium and is not dependent upon upstream history.

Using the "indirect method," the flowfield measurements were further analyzed to extract the turbulent transport terms from the mean flow data. Results show that the variation of the turbulent shear stress τ with distance from the surface is significantly distorted by even modest values of dp/dx. In contrast to the zero pressure gradient distribution, when $dp/dx>0$, τ increases above its wall value, reaching a maximum at y/δ about 0.3-0.4. The normalized shear stress distributor τ/τ_w vs y/δ is independent of the local β_k, although the peak value of τ/τ_w appears to correlate with β_{k0}. The mixing length was calculated from the shear stress distribution and it was found that in the region of the wall, the slope constant k in the expression $\ell/\delta = k/(y/\delta)$ is 0.65 for the adverse pressure gradient case in contrast to the zero pressure gradient value of 0.4. The value of k is independent of β_k and x and is identical to the result obtained by Sturek[6] for $\beta_{k0}=3.45$.

Acknowledgment

This work supported by the U.S. Air Force Aeronautical Systems Division, Wright-Patterson Air Force Base, under Contract F33615-77-C-3016.

References

[1] Fernholz, H. H. and Finley, P. J., "A Critical Compilation of Compressible Turbulent Boundary Layer Data," AGARDograph No. 223, June 1977.

[2] Rubesin, M. W., Crisalli, A. J., Horstman, C. C., and Acharya, M., "A Critique of Some Recent Second Order Closure Models for Compressible Boundary Layers," AIAA Paper 77-128, Jan. 1977.

[3] Mikulla, V. and Horstmann, C. C., "Turbulent Measurements in Hypersonic Shock-Wave Boundary-Layer Interaction Flows," AIAA Paper 76-162, Jan. 1976.

[4] Acharya, M., Kussoy, M. I., and Horstman, C. C., "Reynolds Number and Pressure Gradient Effects on Compressible Turbulent Boundary Layers," AIAA Paper 78-199, Jan. 1978.

[5]Goozait, E. and Childs, M. E., "Turbulence Measurements in Axisymmetric Supersonic Boundary Layer Flow in Adverse Pressure Gradients," AIAA Paper 77-129, Jan. 1977.

[6]Sturek, W. B., "Turbulent Boundary Layer Shear Stress Distributions for Compressible Adverse Pressure Gradient Flow," *AIAA Journal*, Vol. 12, March 1974, pp. 375-376; see also AIAA Paper 73-166, Jan. 1973.

[7]Laderman, A. J., "Pressure Gradient Effects on Supersonic Boundary Layer Turbulence," Ford Aerospace & Communications Corp., Newport Beach, Calif., Rept. U-6467, Oct. 1978.

[8]Laderman, A. J., "Effect of Wall Temperature on a Supersonic Turbulent Boundary Layer," *AIAA Journal*, Vol. 16, July 1978, pp. 723-729.

[9]Clauser, F. H., "The Turbulent Boundary Layer," *Advances in Applied Mechanics*, Vol. 4, Academic Press, New York, 1956, pp. 1-51.

[10]Alber, I. E. and Coats, D. E., "Analytical Investigation of Equilibrium and Non-Equilibrium Compressible Turbulent Boundary Layers," AIAA Paper 69-689, June 1969.

[11]Lewis, J. E., Gran, R. L., and Kubota, T., "An Experiment on the Adiabatic Compressible Turbulent Boundary Layer in Adverse and Favourable Pressure Gradients," *Journal of Fluid Mechanics*, Vol. 51, Pt. 4, 1972, pp. 657-672.

[12]Sturek, W. B. and Danberg, J. E., "Supersonic Turbulent Boundary Layer in an Adverse Pressure Gradient; Data Tabulation," Univ. of Delaware, Dept. of Mechanical and Aerospace Engineering, Tech. Rept. 141, 1973.

[13]Sturek, W. B. and Danberg, J. E., "Supersonic Turbulent Boundary Layer in Adverse Pressure Gradient, Pt. I: Experiment," *AIAA Journal*, Vol. 10, April 1972, pp. 475-480.

[14]Sturek, W. B. and Danberg, J. E., "Supersonic Turbulent Boundary Layer in Adverse Pressure Gradient, Pt. II: Data Analysis," *AIAA Journal*, Vol. 10, May 1972, pp. 630-635.

[15]Coles, D. E., "The Young Person's Guide to the Data," *Proceedings of 1968 AFOSR-IFP-Stanford Conference on Computation of Turbulent Boundary Layers*, Vol. 2, edited by D. Coles and E. Hirst, Stanford Univ., Stanford, Calif., 1969, pp. 1-45.

[16]Van Driest, E. R., "Turbulent Boundary Layer in Compressible Fluids," *Journal of the Aeronautical Sciences*, Vol. 18, 1951, pp. 145-160.

[17]Mathews, D. C., Childs, M. E., and Paynter, G. C., "Use of Coles Universal Wake Function for Compressible Turbulent Boundary Layers," *Journal of Aircraft*, Vol. 7, April 1970, pp. 137-140.

[18]Spalding, D. B., "A Single Formula for the Law-of-the-Wall," *Transactions of ASME, Journal of Applied Mechanics*, Pt. 28E, 1961, pp. 455-457.

[19]Coles, D. E. and Hirst, E. A., *Proceedings of 1968 AFOSR-IFP-Stanford Conference on Computation of Turbulent Boundary Layers*, Vol. 2, Stanford Univ., Stanford, Calif., 1969.

[20]Mellor, G. L. and Gibson, D. M., "Equilibrium Turbulent Boundary Layers," *Journal of Fluid Mechanics*, Vol. 24, 1966, pp. 225-253.

[21]Bradshaw, P. and Unsworth, K., "Comment on 'Evaluation of Preston-Tube Calibration Equations in Supersonic Flow,' " *AIAA Journal*, Vol. 12, Sept. 1974, pp. 1293-1294.

[22]Hopkins, E. J. and Inouye, M., "An Evaluation of Theories for Predicting Turbulent Skin Friction and Heat Transfer on Flat Plates at Supersonic and Hypersonic Mach Numbers," *AIAA Journal*, Vol. 9, Jan. 1971, pp. 993-1003.

[23]Coles, D. E., "The Wall of the Wake in the Turbulent Boundary Boundary Layer," *Journal of Fluid Mechanics*, Vol. 1, 1956, pp. 191-226.

[24]Sandborn, V. A., "A Review of Turbulence Measurements in Compressible Flow," NASA TMX-62337, March 1974.

[25]Maise, G. and McDonald, H., "Mixing Length and Kinematic Eddy Viscosity in a Compressible Boundary Layer," *AIAA Journal*, Vol. 6, Jan. 1968, pp. 73-79.

[26]Bradshaw, P. and Ferris, D. H., "The Response of a Retarded Equilibrium Turbulent Boundary Layer to the Sudden Removal of Pressure Gradient," National Physical Laboratory, Aero. Rept. 1145, 1965.

[27]Glowacki, W. J. and Chi, S. W., "A Study of the Effect of Pressure Gradient on the Eddy Viscosity and Mixing Length for Incompressible Equilibrium Turbulent Boundary Layers," Naval Ordnance Lab., Silver Spring, Md., NOL TR 74-105, May 1974.

[28]Galbraith, R. A. and Head, M. R., "Eddy Viscosity and Mixing Length from Measured Boundary Layer Developments," *Aeronautical Quarterly*, Vol. 26, May 1975, pp. 133-154.

From the AIAA Progress in Astronautics and Aeronautics Series . . .

REMOTE SENSING OF EARTH FROM SPACE: ROLE OF "SMART SENSORS"—v. 67

Edited by Roger A. Breckenridge, NASA Langley Research Center

The technology of remote sensing of Earth from orbiting spacecraft has advanced rapidly from the time two decades ago when the first Earth satellites returned simple radio transmissions and simple photographic information to Earth receivers. The advance has been largely the result of greatly improved detection sensitivity, signal discrimination, and response time of the sensors, as well as the introduction of new and diverse sensors for different physical and chemical functions. But the systems for such remote sensing have until now remained essentially unaltered: raw signals are radioed to ground receivers where the electrical quantities are recorded, converted, zero-adjusted, computed, and tabulated by specially designed electronic apparatus and large main-frame computers. The recent emergence of efficient detector arrays, microprocessors, integrated electronics, and specialized computer circuitry has sparked a revolution in sensor system technology, the so-called smart sensor. By incorporating many or all of the processing functions within the sensor device itself, a smart sensor can, with greater versatility, extract much more useful information from the received physical signals than a simple sensor, and it can handle a much larger volume of data. Smart sensor systems are expected to find application for remote data collection not only in spacecraft but in terrestrial systems as well, in order to circumvent the cumbersome methods associated with limited on-site sensing.

505 pp., 6×9, illus., $22.00 Mem., $42.50 List

TO ORDER WRITE: Publications Dept., AIAA, 1290 Avenue of the Americas, New York, N. Y. 10019